The Mechanism of Metal Cation Binding in Two Nalidixate Calixarene Conjugates. A Langmuir Film and Molecular Modeling Study

ARTICLE *in* THE JOURNAL OF PHYSICAL CHEMISTRY B · AUGUST 2010

Impact Factor: 3.3 · DOI: 10.1021/jp102471c · Source: PubMed

The Mechanism of Metal Cation Binding in Two Nalidixate Calixarene Conjugates. A Langmuir Film and Molecular Modeling Study

Beata Korchowiec,[†,‡] Monika Orlof,[†,‡] Guillaume Sautrey,[‡] Adel Ben Salem,[‡,§] Jacek Korchowiec,[||] Jean-Bernard Regnouf-de-Vains,[‡] and Ewa Rogalska*[,‡]

Department of Physical Chemistry and Electrochemistry, Faculty of Chemistry, Jagiellonian University, ul. R. Ingardena 3, 30-060 Krakow, Poland, Equipe GEVSM, Structure et Réactivité des Systèmes Moléculaires Complexes, UMR 7565 Nancy Université/CNRS, BP 239, 54506 Vandoeuvre-lès-Nancy cedex, France, and Department of Theoretical Chemistry, Faculty of Chemistry, Jagiellonian University, ul. R. Ingardena 3, 30-060 Krakow, Poland

Received: March 18, 2010; Revised Manuscript Received: June 21, 2010

The two new *p-tert*-butylcalix[4]arene derivatives described here bear one or two nalidixic acid arms linked to the lower calixarene rim via the quinolone carboxylate moiety. These derivatives were synthesized in order to investigate two important features of molecules conceived as potential antibiotics, namely, metal cation complexation and interfacial properties, and the way in which they interrelate. The properties of the calixarene derivatives were studied in monomolecular films spread on pure water and on aqueous subphases containing biologically relevant mono- and divalent metal cations. These systems were examined via surface pressure and surface electrical potential measurements, polarization modulation infrared reflection absorption spectroscopy, and molecular modeling. Molecular modeling shows that important differences exist, first, between the structure and stability of the complexes formed with the two derivatives and, second, between their mono- and dication complexes. Correlating the properties of the monolayers with those of the modeled molecules lets us propose that the derivatives bearing one or two nalidixic pending arms form preferentially inter- and intramolecular complexes, respectively. The results obtained in this study indicate that a possible biological role of the nalidixic arms grafted on the calixarene crown may be revealed upon cation complexation.

1. Introduction

Calixarenes, a class of polyphenolic macrocycles, are receiving increased attention due to their great fundamental and practical importance.[1,2] The calix[*n*]arenes can be tailored synthetically by altering the moieties grafted on the aromatic rings. Literature data indicate that calixarene derivatives may be useful as drugs.[3,4] Some derivatives show anti-infectious activity.[5−8]

In our group, different synthetic methods have been developed to prepare calixarene derivatives.[9−14] Some of the ionic calixarene derivatives prepared were active against Gram-positive as well as Gram-negative bacteria.[15] The derivatives bearing antibiotic moieties[9,10,12] were conceived as possible drug carriers, releasing the antibiotic upon hydrolysis, as demonstrated in a biological medium with water-soluble ionic species.[12] It can be expected that the antibiotics can be released from water-insoluble derivatives as well. The choice of *p-tert*-butyl calixarene was directly related to a possible application of the molecules studied as prodrugs. An oral administration would lead to the release of the soluble antibacterial agent in the intestinal compartment; the insoluble, nontoxic calixarene molecule could be thus easily eliminated from the organism. We want to note that some water-soluble calixarene derivatives obtained in our laboratory, which are active as antibacterials, are polyionic species, and thus are not suitable for oral administration.

The calixarenes used in the present study (Figure 1) belong to the group of *p-tert*-butylcalix[4]arene-based podands, bearing one or two[9] nalidixic arms linked to the lower rim of the calixarene platform via a carboxylate function present in the quinolone moiety. These derivatives were synthesized with the aim of deepening the understanding of two important features of these derivatives, namely, metal cation complexation and interfacial properties, and their interrelationship.

Quinolones, which potentially offer many of the attributes of ideal antibiotics, have been the center of considerable scientific and clinical interest since their discovery in the early 1960s. Nalidixic acid was the first quinolone available for clinical use.[16] It was proposed in the literature that the incorporation of quinolones into cells occurs via a simple diffusion mechanism.[17] It can be noticed that simple diffusion depends on the amphiphilicity of the molecule. Consequently, it is not astonishing that the quinolones in zwitterionic form exhibited high permeation, whereas the uptake was strongly reduced when the drug carried a net charge as a result of ionization or complex formation with divalent ions.[18] Interestingly, the latter effect was not observed with monovalent cations. It was proposed that the metal cations were chelated by the 4-oxo and adjacent carboxyl groups. Since these functional groups are required for antibacterial activity, it could be expected

* Corresponding author. E-mail: rogalska@uhp-nancy.fr. Phone: +33 (0)3 83 68 43 45. Fax: +33 (0)3 83 68 43 22.
[†] Department of Physical Chemistry and Electrochemistry, Jagiellonian University.
[‡] Nancy Université.
[§] Current address: Laboratoire de Chimie Appliquée: Hétérocycles, Corps Gras et Polymères. Département de Chimie, Faculté des Sciences de Sfax, 3000 Sfax, B.P. 1171, Tunisia.
[||] Department of Theoretical Chemistry, Jagiellonian University.

10.1021/jp102471c
Published on Web 07/26/2010

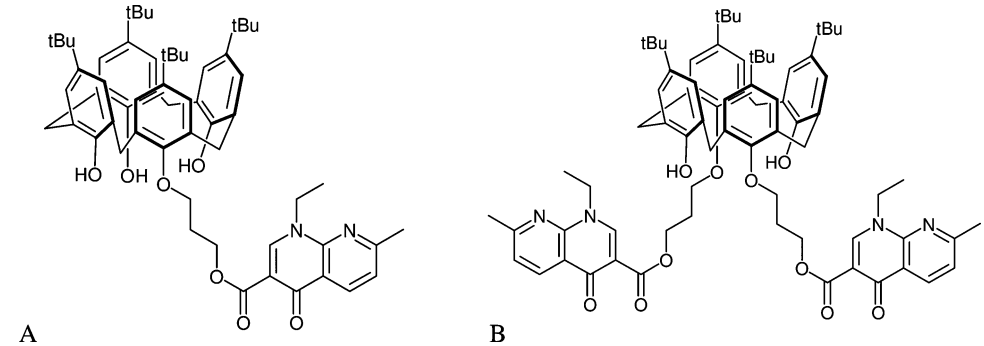

Figure 1. Calixarene derivatives: *p-tert*-butylcalix[4]arene-monopropylnalidixate (A; calix I) and *p-tert*-butylcalix[4]arene-bis-propylnalidixate (B; calix II).

that all quinolones interact with metal ions. However, there are indications that differences may exist between different quinolones regarding the detailed mechanism of interaction with cations.[18,19]

The complexation and membrane-related characteristics of calixarene derivatives can be studied simultaneously using the Langmuir film technique. Indeed, it was shown that complexation of metal ions affects the monolayer properties and can be correlated with the macrocycle-cation selectivity.[1,2,20−25] Moreover, the Langmuir film technique allows studying of the behavior of amphiphilic macrocycles in a lipid environment.[26,27] Importantly, the amphiphilicity of calixarenes can be adjusted by grafting lateral chains of different structure to the crown. The fact that the two derivatives differ by the number of the grafted nalidixic acid moieties permits estimating an additive thermodynamic contribution of pendant arms to the complexation of the cations. The latter effect was described in the literature in the case of the calixarene derivatives bearing a variable number of (ethylethanoate)oxy or ethylthioethoxy arms complexing Hg^{2+} in acetonitrile.[28]

Here, the properties of the new calixarene derivatives were studied in monomolecular films spread at the air−aqueous interface, using the Langmuir technique. Surface pressure−molecular area ($\Pi-A$) isotherms, surface potential−molecular area ($\Delta V-A$) isotherms, and polarization-modulation infrared reflection−absorption spectroscopy (PM-IRRAS) were used to characterize the monolayers. The monolayers were formed on a pure water subphase and on solutions of mono- and divalent metal chlorides: LiCl, NaCl, KCl, $MgCl_2$, $CaCl_2$, $BaCl_2$, $ZnCl_2$, and $CuCl_2$. The compression isotherms were also determined as a function of salt concentration, using aqueous solutions of salts in the range 5×10^{-6} to 5×10^{-2} M. On the other hand, molecular modeling of free ligands and metal cation complexes allowed a reliable interpretation of the experimental results in terms of conformational rearrangement of these molecules upon complexation, and stability of the complexes formed. The overall results may be useful when designing new synthetic calixarene-based drugs and for understanding how these molecules interact with the cell membranes. The results obtained gave us insight into the inter- and intramolecular interactions of these molecules and showed that the calixarenes studied differ significantly in their interfacial behavior. This study prepares the ground for further research on the biological activity of calixarene−antibiotic conjugates.

2. Experimental Section

Molecular Modeling. All calculations have been performed with the Gaussian 03 suite of programs.[29] The Becke three-parameter exchange functional in combination with the Lee−Yang−Parr correlation functional, i.e., the B3LYP hybrid functional, was applied. The basis set of double-ζ quality (6-31G*) with polarization functions on heavy atoms was used in calculations.

Materials and Reagents. Analytical grade LiCl, NaCl, KCl, $CaCl_2\times2H_2O$, $BaCl_2\times2H_2O$, $MgCl_2\times6H_2O$, $ZnCl_2$, and $CuCl_2\times2H_2O$ were from Sigma-Aldrich. Spectrophotometric grade chloroform (purity ≥99.8%) used for preparing calibrated calixarene derivative solutions was from Sigma-Aldrich. Milli-Q water, which had a surface tension of 72.8 mN m^{-1} at 20 °C, pH 5.6, was used in all experiments. The pH of 5×10^{-2} M salt solutions at 20 °C was 6.7 (LiCl), 5.9 (NaCl), 6.5 (KCl), 5.6 ($CaCl_2$), 5.8 ($BaCl_2$), 6.4 ($MgCl_2$), 6.8 ($ZnCl_2$), and 4.2 ($CuCl_2$).

Synthesis. Calix II was synthesized as described previously.[9] Calix I was synthesized as follows. A mixture of *p-tert*-butylcalix[4]arene (0.5 g, 0.77×10^{-3} mol), $NaHCO_3$ (0.088 g, 1.04×10^{-3} mol), bromopropylnalidixic ester (0.229 g, 0.65×10^{-3} mol), and KI (0.3 g) in anhydrous MeCN (100 mL) was maintained at reflux under anhydrous conditions for 24 h. The solvent was evaporated to dryness, and the residue was dissolved in CH_2Cl_2, washed with H_2O, and dried over Na_2SO_4. After concentrating, the organic phase was cooled to 4 °C and the resulting precipitate was filtered off. The filtrate was finally chromatographed (Chromatotron, SiO_2, CH_2Cl_2/CH_3OH; 10:0.2) to give calix I (0.25 g; 35%).

M.p.: 132 °C. IR (KBr): 1696.43 (CO); 1736.03 (COO). UV−vis (CH_2Cl_2): 259 (27841); 281 (22170); 329 (14084); 337(14473). ^{1}H NMR: 1.21 (s, 9 H, Me_3C); 1.23 (s, 18 H, Me_3C); 1.25 (s, 9 H, Me_3C); 1.46 (t, $J = 7.24$ Hz, 3 H, CH_3CH$_2$); 2.63, 2.66 (s+qunt, 5 H, CH_3 + OCH$_2$CH_2CH$_2$OCO); 3.43, 4.30 (1/2AB, $J_{AB} = 12.4$ Hz, 4 H, ArCH_2Ar); 3.46, 4.41 (1/2AB, $J_{AB} = 13.35$ Hz, 4 H, ArCH_2Ar); 4.39 (q, $J = 4.391$ Hz; 2 H, CH_2CH$_3$); 4.43 (t, $J = 7.44$ Hz, 2 H, OCH_2CH$_2$CH$_2$OCO); 4.84 (t, $J = 6.1$ Hz, 2 H, OCH$_2$CH$_2$CH_2OCO); 7.01 (AX, $J = 2.48$ Hz, 2 H, Ar*H*); 7.06 (AX, $J = 2.48$ Hz; 2 H, Ar*H*); 7.07 (s, 2 H, Ar*H*); 7.10 (s, 2 H, Ar*H*); 7.25 (d, $J = 8.01$ Hz, 1 H, *H*(6)); 8.66 (d, $J = 8.01$ Hz, 1H, *H*(5)); 8.73 (s, 1 H, *H*(2)); 9.54 (s, 2 H, O*H*); 10.11 (s, 1 H, O*H*). ^{13}C NMR ($CDCl_3$): 15.57 (*C*H$_3$CH$_2$); 25.44 (*C*H$_3$); 29.71 (OCH$_2$*C*H$_2$CH$_2$OOC); 31.43 (*Me*$_3$C); 32.09 (*Me*$_3$C); 32.53 (Ar*C*H$_2$Ar); 34.17 (Me$_3$*C*), 34.37 (Me$_3$*C*); 46.89 (CH$_3$*C*H$_2$); 61.95 (OCH$_2$CH$_2$*C*H$_2$OCO); 72.93 (O*C*H$_2$CH$_2$CH$_2$OCO); 112.34 (*C*(3)); 121.22 (*C*(6)); 121.73 (*C*(9)); 125.43, 125.99 (C_m of Ar); 127.98, 133.15 (C_o of Ar); 137.06 (*C*(5)); 141.74, 147.32 (C_p of Ar); 149.18 (*C*(2)); 148.96 (*C*(7)); 150.00, 151.16 (C_i of Ar); 162.78 (*C*(10)); 165.51 (OCH$_2$CH$_2$CH$_2$OO*C*); 175.12 (*C*(4)). Anal. Calcd for $C_{57}H_{72}O_7N_2$ (921.21): C 76.92, H 7.88, N 3.04; found: C 76.70,

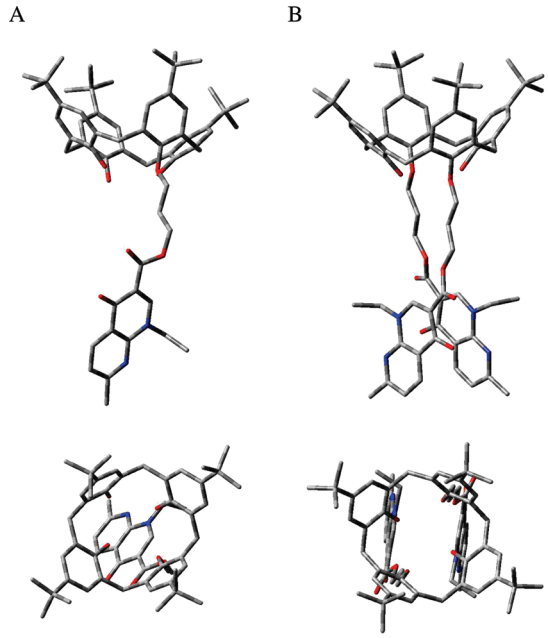

Figure 2. Gas phase optimized structures of the free calix I (A) and calix II (B) ligands. Upper and bottom line: side and top views, respectively. The hydrogen atoms were omitted for clarity. Color code: carbons in gray, oxygens in red, nitrogens in blue.

H 7.88, N 3.26. ES-MS (pos. mode): 921.39 (100), 922.41 (75), 923.42 (35), 924.38 (10) $[\mathbf{M}+\mathrm{H}]^+$.

Compression Isotherms. The surface pressure (Π) and electric surface potential (ΔV) measurements were carried out with a KSV 5000 Langmuir balance (KSV Instruments Ltd., Helsinki, Finland). A Teflon trough (15 cm × 58 cm × 1 cm) with two hydrophilic Delrin barriers (symmetric compression) was used in compression isotherm experiments. The system was equipped with an electrobalance and a platinum Wilhelmy plate (perimeter 3.94 cm) as a surface pressure sensor. The surface potential was measured using a KSV Spot 1 with a vibrating plate electrode and a steel counter electrode immersed in the subphase. The apparatus was enclosed in a Plexiglas box, and the temperature was kept constant at 20 °C. All solvents used for cleaning the trough and the barriers were of analytical grade. Aqueous subphases for monolayer experiments were prepared with Milli-Q water. Monolayers were spread on pure water using calibrated solutions (concentration about 0.5 mg mL^{-1}) of pure calixarenes. After an equilibration time of 20 min, the films were compressed at a rate of 2.5 mm min^{-1} $barrier^{-1}$ by two symmetrically moving barriers. A PC computer and KSV software were used to control the experiments. Each compression isotherm was performed at least three times. The standard deviation was ±0.5 $Å^2$ for mean molecular area (A), ±0.2 mN m^{-1} for surface pressure, and ±0.005 V for surface potential measurements. The compression isotherms allowed calculating the compressibility modulus (C_S^{-1}; $C_S^{-1} = -A(\partial\Pi/\partial A)_T$) and the effective dipole moment ($\mu_{eff;}$ $\Delta V = \mu_{eff}/\varepsilon_0\varepsilon A$, where A is the area per molecule, ΔV is the surface potential corresponding to A, ε_0 is the permittivity of a vacuum, and ε is the permittivity of a monolayer, which is assumed to be 1).[30,31] The collapse parameters ΔV_{coll}, Π_{coll}, and A_{coll} were determined directly from the compression isotherms.

Polarization-Modulation Infrared Reflection−Absorption Spectroscopy. The PM-IRRAS spectra of the monolayers spread on pure water or on salt solutions were registered at 20 °C. The Teflon trough dimensions were 36.5 cm × 7.5 cm × 0.5 cm; other experimental conditions were described elsewhere.[32] The PM-IRRAS measurements were performed using a KSV PMI 550 instrument (KSV Instruments Ltd., Helsinki, Finland). Half-wave retardations of 1500 and 2900 cm^{-1} were used for analyzing the methylene and carbonyl regions of the spectra, respectively. The spectral range of the device is 800−4000 cm^{-1}, and the resolution is 8 cm^{-1}. More information concerning the PM-IRRAS device can be found in a precedent paper.[32]

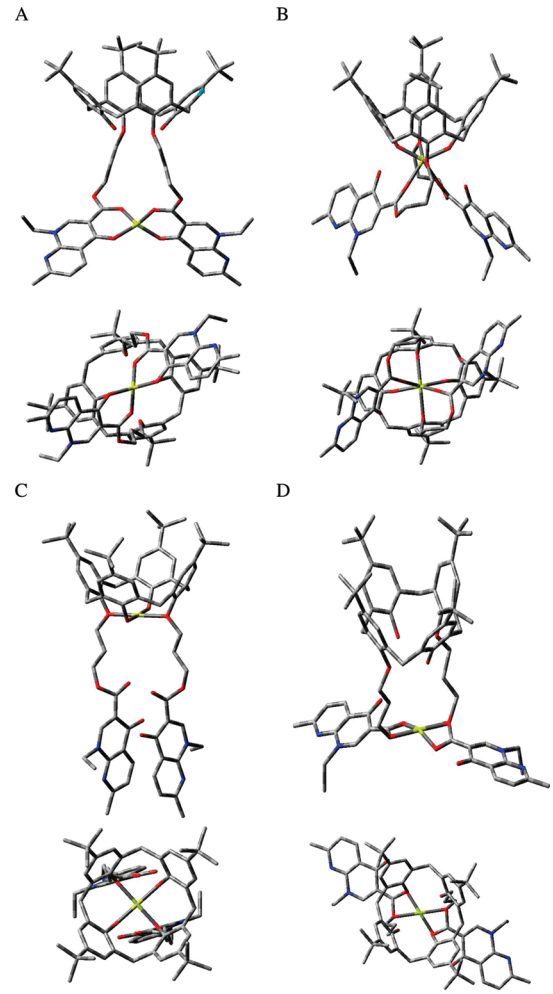

Figure 3. Side and top views of four different structures of Li^+−calix II located at the B3LYP/6-31G* level of theory. The hydrogens were removed for clarity. Color code: carbons in gray, oxygens in red, nitrogens in blue, Li^+ in yellow.

3. Results and Discussion

The Langmuir technique was used for differentiating between two structurally closely related calixarene derivatives and for quantifying the interaction between the two derivatives and metal cations. To this end, surface pressure and surface potential measurements as well as PM-IRRAS experiments were performed. Modeling of the free ligands and chosen complexes allowed a better understanding of the experimental results.

Molecular Modeling. The geometrical structures of both ligands are shown in Figure 2. In the case of calix I, several local minima resulting from rotation around the C−C bonds in the nalixidic acid−calixarene linker can be expected. Such

TABLE 1: Interaction Energies ($E_{INT} = E_{X-calix} - E_{calix} - E_X$) Obtained at the B3LYP/6-31G* Level of Theory for the Lowest Energy X−Calix Systems, Where X = Li^+, Na^+, K^+, Mg^{2+}, Ca^{2+}, Zn^{2+}, and Cu^{2+}, Respectively (All Values Are in kJ mol^{-1})

	Li^+	Na^+	K^+	Mg^{2+}	Ca^{2+}	Zn^{2+}	Cu^{2+}
				Gas Phase			
calix I[a]	−501.6	−356.7	−241.2	−1456.2	−1083.5	−1647.5	−1732.5
calix II[b]	−612.9	−479.0	−358.8	−1614.4	−1182.8	−1834.7	−1911.3
	−524.2	−431.7	−290.1	−1595.2	−1241.4	−1770.6	−1820.0
				Polarizable Continuum Model			
calix I[a]	−15.7	16.1	21.7	−82.8	66.0	−96.2	−550.4
calix II[b]	−111.8	−83.6	−58.3	−220.4	−68.1	−272.6	−716.4
	4.9	0.9	42.3	−99.7	34.1	−112.7	−538.1

[a] Structures presented in Figure 4. [b] Structures presented in Figure 3A and B (upper and bottom line, respectively).

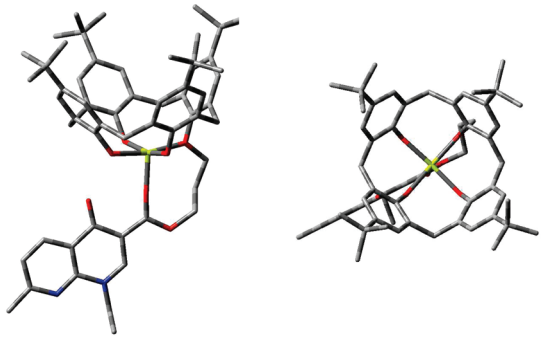

Figure 4. Side and top views of the Li^+−calix I structure located at the B3LYP/6-31G* level of theory. The hydrogens were removed for clarity. Color code: carbons in gray, oxygens in red, nitrogens in blue, Li^+ in yellow.

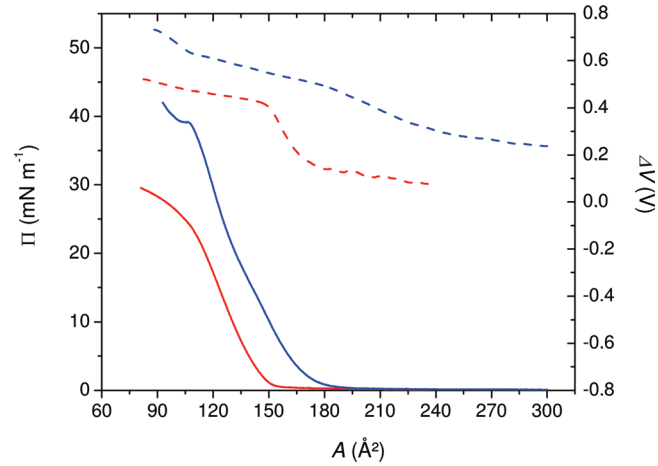

Figure 5. Compression isotherms of calix I (red line) and calix II (blue line) spread on pure water at 20 °C; pH 5.6. Π−*A* isotherms, solid lines; Δ*V*−*A* isotherms, dotted lines.

rotations are not observed in the more rigid calix II, which is stabilized by the intramolecular nalidixic residue interaction. Both derivatives have local basic sites, namely, the calixarene lower rim hydroxyl oxygens and the nalidixic moiety heteroatoms. While oxygens can form coordination bonds with cations, the nitrogen atoms are not taken into consideration due to a steric hindrance. In the case of small cations (Li^+ and Mg^{2+}), four different symmetric complexes with calix II were located. Figure 3 shows the structures of the Li^+−calix II complexes in the order of decreasing stabilization energy (absolute value). The complexes shown in Figure 3A, C, D, and B have coordination numbers equal to 4 and 6, respectively.

The calix II complexes with coordination analogous to that shown in Figure 3A and B were located for all cations except Ba^{2+}; for convergence reasons, calculations could not be done in the latter case. In Table 1 are listed the interaction energies: $E_{INT} = E_{X-calix} - E_{calix} - E_X$, where X−calix, calix, and X are the complex, the base (calixarene derivative), and the acid (mono- or divalent cation), respectively. It can be seen that all complexes are thermodynamically stable ($E_{INT} < 0$). With the exception of the Ca^{2+}−calix II complex, the structure shown in Figure 3A is the most stable. The most stable are the monocation Li^+−calix II complexes, while the least stable are K^+−calix II. For dicationic complexes, the following gas phase stability sequence was obtained: $|E_{INT}(Ca^{2+}-calix\ II)| < |E_{INT}(Mg^{2+}-calix\ II)| < |E_{INT}(Zn^{2+}-calix\ II)| < |E_{INT}(Cu^{2+}-calix\ II)|$. The complexes formed with dications are more stable compared to monocations. The same trends are observed for the X−calix I complexes (Table 1). The structure of the Li^+−calix I complex is shown in Figure 4. The structures of other complexes are similar to Li^+−calix I; the coordination number of all complexes is 5. A complex formed by binding a cation to the calixarene lower rim hydroxyl oxygens could possibly be located. However, such complexes are expected to be less stable than those presented in Figure 4 and Table 1. The Li^+−calix II complex shown in Figure 3C is ∼105 kJ mol^{-1} less stable than that shown in Figure 3B; in the case of Mg^{2+}−calix II, which is a complex formed with a dication, this difference is 335 kJ mol^{-1}.

The data reported in Table 1 correspond to the gas phase. Therefore, it is always an open question whether the order of conformers observed in the gas phase will be preserved in solution. Since the discrete model of the solution practically cannot be applied due to the system size, we have performed calculations using the polarizable continuum model (PCM). The cavity was created using the van der Waals surface and UFF radii. The results are listed in Table 1. The geometries of all systems were not reoptimized (single point calculations); therefore, the results have qualitative character. One can notice that the complexes analogous to this shown in Figure 3A are thermodynamically stable. The same stability sequence as for the gas phase is observed: $|E_{INT}(K^+-calix\ II)| < |E_{INT}(Na^+-calix\ II)| < |E_{INT}(Li^+-calix\ II)|$ and $|E_{INT}(Ca^{2+}-calix\ II)| < |E_{INT}(Mg^{2+}-calix\ II)| < |E_{INT}(Zn^{2+}-calix\ II)| < |E_{INT}(Cu^{2+}-calix\ II)|$. All energies are lower than the corresponding gas phase energies (see Table 1). The energy lowering for the Cu^{2+}−calix II system is not so pronounced as for the remaining systems. The second conformers of calix II are thermodynamically stable only with Mg^{2+}, Zn^{2+}, and Cu^{2+}. The complexes with Ca^{2+} and all monocations are unstable. In a case of calix I, the complexes with Na^+, K^+, and Ca^{2+} are unstable while with Li^+, Mg^{2+}, Zn^{2+}, and Cu^{2+} are stable. The stability/instability sequence is in agreement with gas phase data.

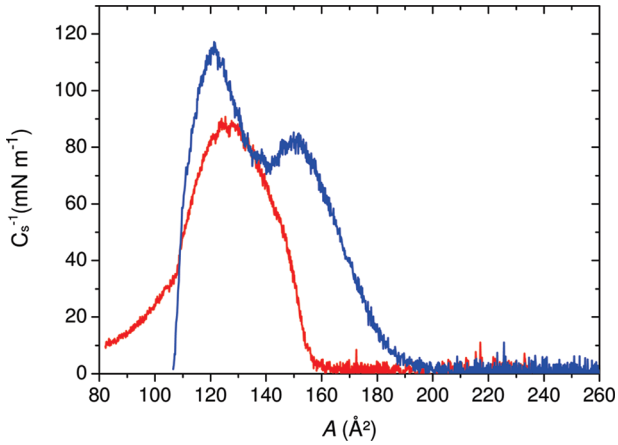

Figure 6. Compressibility analysis of calix I (red line) and calix II (blue line) monolayers spread on pure water at 20 °C; pH 5.6.

TABLE 2: Characteristic Parameters of the Compression Isotherms Obtained on Pure Water

	A_{coll} (Å^2)	Π_{coll} (mN m^{-1})	$Cs^{-1}{}_{max}$ (mN m^{-1})	ΔV_{coll} (V)	$\mu_\perp$ (D)
calix I	125	13.5	90.8	0.45	1.49
calix II	121	28.4	117.2	0.61	1.96

Because the pendant arm in calix I is flexible, formation of complexes with two neighbor calixarene molecules and dications can be expected. The data obtained for X−calix II showing that both pendant arms participate in the complexation support this conjecture. Unfortunately, the size of the system does not allow performing geometry optimization of the two-ligand complexes.

Monomolecular Films Formed on Pure Water. As shown in Figures 5 and 6 and in Table 2, the monolayers formed with the two derivatives have different properties. Indeed, the monolayer formed with calix II is more stable and more solid-like, as indicated by a higher value of the surface pressure at the collapse point (Π_{coll}) (Figure 5) and a higher value of the compressibility modulus at the collapse point ($Cs^{-1}{}_{max}$) (Figure 6). A liquid expanded−liquid condensed (LE−LC) phase transition can be observed at around 140 Å^2 with calix II on the $\Pi-A$ isotherms (Figure 5); it shows much more clearly in the $Cs^{-1}{}_{max}-A$ dependencies, obtained by calculating the first derivative of the $\Pi-A$ isotherms (Figure 6, blue line). The film formed with calix I has a liquid expanded character even in the most condensed states, and contrary to calix II, no phase transition can be observed in $Cs^{-1}{}_{max}-A$ (Figure 6, red line).

A slightly higher value of the molecular area at the collapse of the film (A_{coll}) observed with calix I compared to calix II together with a lower value of the surface potential at the collapse of the film (ΔV_{coll}) and of the corresponding dipole moment ($\mu_\perp$) indicate that calix I is more tilted relative to the normal to the water surface than calix II. The computed absolute values of calix I and calix II dipole moments ($|\vec{\mu}|$) are 6.95 D (10.18 D) and 1.31 D (2.59 D), respectively; the values in parentheses were obtained using the PCM model. Due to the assumed symmetry of calix II, the dipole vector lies on the C_2 axis. In calix I, the projection on the axis going through the middle of the calixarene aromatic crown is 1.14 D (0.66 D). However, while the experimental gas phase values of μ may be compared with the PCM values (the length of μ for calix II in the gas phase is shorter compared to the experimental $\mu_\perp$), such comparison is delicate, because the geometry of both ligands was frozen during PCM calculations.

In conclusion to this paragraph, it can be said that the two hydrophilic pending arms present in calix II allow a more vertical orientation of the molecules relative to the water surface, a more regular organization of the molecules at the interface, and, consequently, formation of a more stable and more solid-like monolayer, with a clearly observed LE−LC phase transition, compared to calix I bearing one pending arm.

Monomolecular Films Formed on Salt Solutions. The interactions between calix I or calix II and metal cations were studied in the monolayers spread on LiCl, NaCl, KCl, $MgCl_2$, $CaCl_2$, $BaCl_2$, $ZnCl_2$, and $CuCl_2$ solutions. The results obtained are shown in Tables 3 and 4 and, for chosen cations, in Figure 7. In the case of the $\Pi-A$ isotherms, the most significant differences between pure water and the subphases containing cations are observed in the case of transition metals (Cu^{2+} and Zn^{2+}). The latter effect can be easily explained on the basis of modeling. Indeed, both calix I and calix II form more stable complexes with the transition metal dications compared to the alkali earth metal dications, which in turn form more stable complexes than the alkali metal monocations; it can be expected that the number of complexed ligands in the film is proportional to the stability of the complexes for a given calixarene derivative. The mixture of rigid complexes and conformationally labile free ligands may be less well packed in the films compared to pure ligands and thus show higher molecular areas. This proposal is supported by the results obtained on the subphases containing increasing concentrations of salts. Indeed, in the case of calix II, the isotherms are shifted to higher molecular areas with the increasing salt concentration, which can be explained by an increasing proportion of the complexed to free ligands in the film. On the other hand, it can be imagined that the monosubstituted calix I forms intermolecular complexes between neighbor ligands, which can lead to the condensation of the film at higher cation concentrations. This effect is well seen with Ca^{2+}−calix I (Figure 7C); it was not observed with the bisubstituted calix II, which forms intramolecular complexes of a higher stability than calix I (Table 1). It can be supposed that the more important shifts of the $\Pi-A$ isotherms obtained on pure water and on the salt subphase observed in the case of calix I are due to a higher compressibility of the film compared to calix II. It can be observed that the $\Delta V-A$ isotherms are sensitive tools for revealing complexation. The higher values of the surface potential and dipole moment (Figure 7 and Tables 3 and 4) in complexes compared to pure water can be explained by a more vertical orientation of the former and by the presence of ions at the interface; the surface concentration of the ions would be higher in the case of the more stable complexes (Table 1).[33,34] On the other hand, as observed by the anonymous reviewer, the $\Pi-A$ plots obtained on pure water or on the KCl are similar, while the $\Delta V-A$ plots are different. The latter suggests that not only orientation of the molecules but also formation of the complex and the presence of the ion at the interfacial region influence the measured surface potential.[35]

PM-IRRAS. While the interfacial properties and mechanism of action of molecules such as phosphoglycerides and proteins have been intensively studied using PM-IRRAS over the last years,[36−38] this approach was rarely used with molecules resulting from organic synthesis,[39,40] such as macrocycles.[41] A more detailed knowledge at the atomic level of the behavior of calixarene derivatives may be important from the point of view of fundamental research and for possible applications. Here, the characteristic calixarene

TABLE 3: Characteristic Parameters of the Compression Isotherms Obtained with Calix I at Different Salt Concentrations in the Subphase

subphase	conc (M)	A_{coll} (Å^2)	Π_{coll} (mN m^{-1})	$Cs^{-1}{}_{max}$ (mN m^{-1})	ΔV_{coll} (V)	$\mu_\perp$ (D)
LiCl	5×10^{-6}	117	23.3	111.7	0.47	1.46
	5×10^{-3}	111	24.1	105.3	0.50	1.47
	5×10^{-2}	111	25.4	106.6	0.52	1.54
NaCl	5×10^{-6}	115	23.1	103.8	0.49	1.50
	5×10^{-3}	112	24.3	103.6	0.51	1.52
	5×10^{-2}	111	25.2	104.6	0.52	1.54
KCl	5×10^{-6}	112	22.9	106.9	0.49	1.46
	5×10^{-3}	107	24.0	103.5	0.51	1.45
	5×10^{-2}	106	25.3	102.9	0.52	1.46
$MgCl_2$	5×10^{-6}	110	23.5	106.5	0.50	1.51
	5×10^{-3}	107	24.2	99.9	0.54	1.52
	5×10^{-2}	98	25.1	107.7	0.56	1.46
$CaCl_2$	5×10^{-6}	114	22.2	102.0	0.47	1.42
	5×10^{-3}	106	24.9	100.8	0.53	1.48
	5×10^{-2}	101	25.9	104.1	0.54	1.47
$BaCl_2$	5×10^{-6}	105	24.0	105.8	0.49	1.37
	5×10^{-3}	99	25.7	110.1	0.54	1.41
	5×10^{-2}	95	27.1	99.2	0.55	1.39
$CuCl_2$	5×10^{-6}	117	23.0	113.8	0.48	1.49
	5×10^{-3}	117	24.4	120.2	0.50	1.55
	5×10^{-2}	119	24.9	132.5	0.53	1.68
$ZnCl_2$	5×10^{-6}	114	23.2	111.1	0.47	1.44
	5×10^{-3}	112	26.7	106.0	0.52	1.54
	5×10^{-2}	105	27.4	105.8	0.54	1.57

TABLE 4: Characteristic Parameters of the Compression Isotherms Obtained with Calix II at Different Salt Concentrations in the Subphase

subphase	conc (M)	A_{coll} (Å^2)	Π_{coll} (mN m^{-1})	$Cs^{-1}{}_{max}$ (mN m^{-1})	ΔV_{coll} (V)	$\mu_\perp$ (D)
LiCl	5×10^{-6}	112	38.0	128.5	0.64	1.90
	5×10^{-3}	114	38.3	136.6	0.67	2.04
	5×10^{-2}	114	38.4	124.5	0.69	2.09
NaCl	5×10^{-6}	110	38.0	147.0	0.64	1.86
	5×10^{-3}	111	38.5	130.2	0.67	1.97
	5×10^{-2}	111	38.9	129.5	0.69	2.03
KCl	5×10^{-6}	112	37.1	143.7	0.64	1.90
	5×10^{-3}	111	37.9	130.4	0.66	1.95
	5×10^{-2}	111	38.3	135.8	0.68	2.02
$MgCl_2$	5×10^{-6}	111	38.0	142.8	0.65	1.91
	5×10^{-3}	110	38.4	145.3	0.67	1.95
	5×10^{-2}	109	38.9	134.1	0.67	1.94
$CaCl_2$	5×10^{-6}	111	37.9	125.2	0.65	1.90
	5×10^{-3}	110	38.3	118.4	0.68	2.00
	5×10^{-2}	111	38.5	121.7	0.70	2.06
$BaCl_2$	5×10^{-6}	110	38.4	144.4	0.63	1.82
	5×10^{-3}	109	38.6	153.5	0.68	1.97
	5×10^{-2}	109	38.8	124.3	0.69	2.00
$CuCl_2$	5×10^{-6}	111	38.3	134.9	0.65	1.90
	5×10^{-3}	111	38.6	126.2	0.66	1.96
	5×10^{-2}	116	38.9	123.5	0.69	2.14
$ZnCl_2$	5×10^{-6}	112	38.1	117.7	0.65	1.92
	5×10^{-3}	112	38.4	112.0	0.65	1.94
	5×10^{-2}	117	38.4	103.7	0.65	2.02

derivative bands were observed in the films formed on pure water (Figure 8 and Table 5) and on subphases containing KCl, $CaCl_2$, or $CuCl_2$ (Table 5).

As described in the literature, for groups involved in H-bonding to water, the stretching mode absorption bands shift to lower frequency, whereas bending mode absorption bands shift to higher frequency, as H-bonding increases and entropy decreases.[42,43] In our work, the stretching mode absorption band characteristic for the ester C═O moieties present in calix I and calix II were useful for monitoring the interaction with metal cations in Langmuir films. Indeed, the $\nu(C{=}O)_{ester}$ band is observed in the film spread on pure water at 1733 cm^{-1} (calix I) and at 1737 cm^{-1} (calix II); the $\nu(C{=}O)_{ketone}$ band is observed at 1697 cm^{-1} (calix I) and at 1701 cm^{-1} (calix II), respectively. The shift of the $\nu(C{=}O)_{ester}$ and $\nu(C{=}O)_{ketone}$ bands to higher wavenumbers in the presence of metal cations indicates that cation complexation occurs with a concomitant dehydration of both types of C═O groups. It can be observed that the blue shift is more pronounced for the dications (Table 5). The latter result is in accordance with molecular modeling, indicating that, first, the dication complexes are more stable compared to those formed with monocations and, second, calix II complexes, shown in Figure 3A, as well as two-ligand calix I complexes with divalent cations can be formed.

It is well-known that the wavenumbers of the CH_2 symmetric and antisymmetric modes can be used to monitor the degree of conformational order of alkyl chains. When the hydrocarbon chain is highly ordered (trans-zigzag conformation), the bands

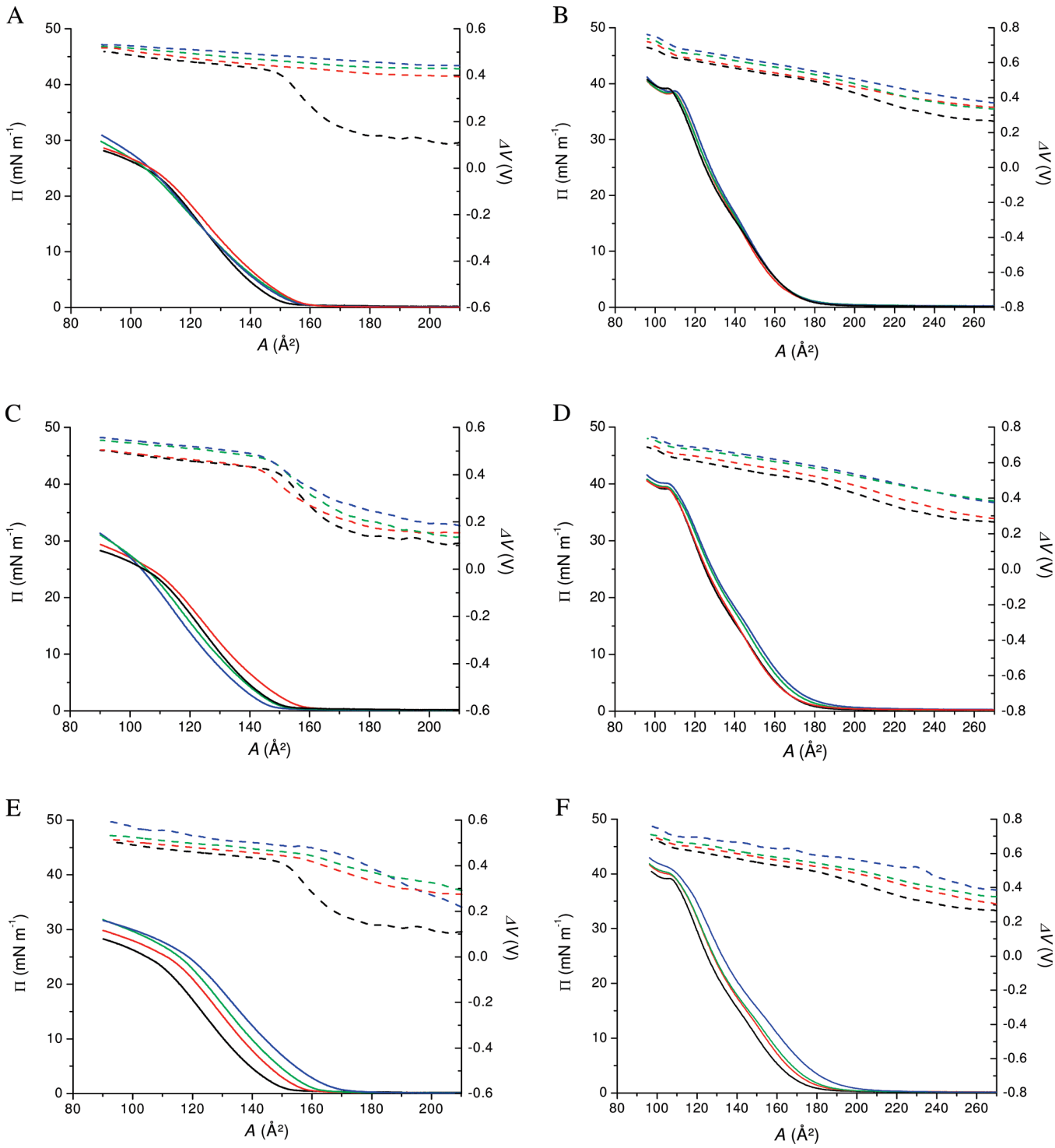

Figure 7. Compression isotherms of the films formed with calix I (A, C, E) and calix II (B, D, F) on KCl (A, B), $CaCl_2$ (C, D), and $CuCl_2$ (E, F) solutions at 20 °C. Π−*A* isotherms, solid lines; Δ*V*−*A* isotherms, dotted lines. Concentration: pure water (black), 5×10^{-6} M (red), 5×10^{-3} M (green), 5×10^{-2} M (blue).

due to CH_2 symmetric and antisymmetric modes appear at around 2850 and 2920 cm^{-1}, respectively. If gauche conformers (conformational disorder) are induced in the alkyl chains, these bands shift to higher frequencies.[44−49]

Here, in the case of films spread on pure water, the bands of the linker CH_2 groups appear at 2863 and 2929 cm^{-1} (calix I) and at 2864 and 2931 cm^{-1} (calix II). These bands shift to lower wavenumbers in the presence of metal cations, except the calix I/KCl system, where $\nu_s(CH_2)$ shifts to a slightly higher value (2871 cm^{-1}) (Table 5). These results indicate ordering of the linkers upon the complexation of both mono- and dications in the case of calix II. In the case of calix I, ordering of the linkers is observed more clearly in the case of the divalent cations. Interestingly, the CH_3 stretching bands characteristic for the calixarene *tert*-Bu moieties are sensitive to dication complexation (Table 5). Indeed, in the presence of dications, both $\nu_s(CH_3)$ and $\nu_{as}(CH_3)$ shift to lower wavenumbers with calix II, while with calix I the shift of $\nu_s(CH_3)$ is observed; such shift is not seen in the presence of K^+. While presently we cannot account for this effect, it can be supposed that it is related to

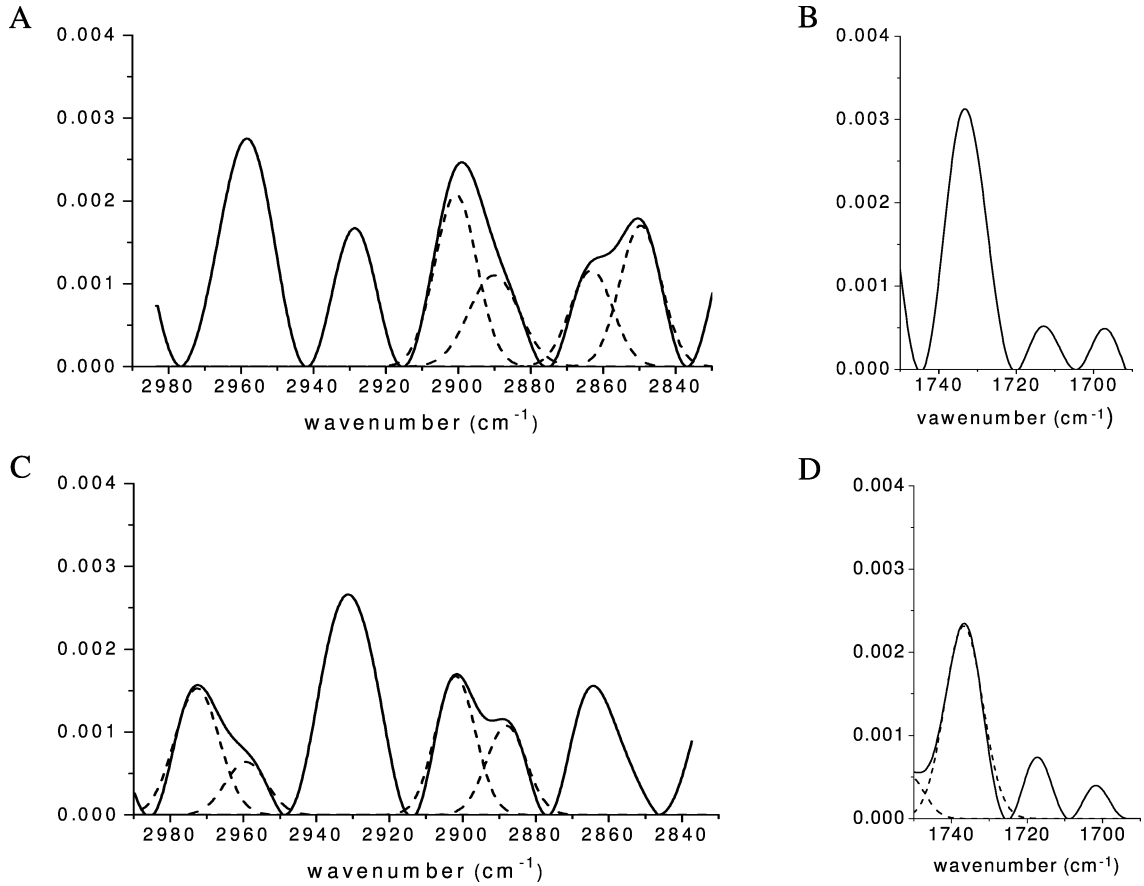

Figure 8. PM-IRRAS spectra of calix I (A, B) and calix II (C, D) spread on a pure water subphase. Surface pressure 30 mN m^{-1}; temperature 20 °C; pH 5.6. Solid lines, experimental spectra; dashed lines, deconvoluted bands.

TABLE 5: Characteristic Vibrational Wavenumbers of the Films Formed with Calix I and Calix II on Pure Water and on Salt Subphases.

	$\nu_s(CH_2)$ (cm^{-1})	$\nu_{as}(CH_2)$ (cm^{-1})	$\nu_s(CH_3)$ (cm^{-1})	$\nu_{as}(CH_3)$ (cm^{-1})	$\nu(C{=}O)_{ester}$ (cm^{-1})	$\nu(C{=}O)_{ketone}$ (cm^{-1})
calix I/water	2863	2929	2890	2959	1733	1697
calix I/KCl	2871	2926	2890	2955	1734	1700
calix I/$CaCl_2$	2856	2919	2877	2960	1735	1698
calix I/$CuCl_2$	2850	2918	2871	2959	1744	1701
calix II/water	2864	2931	2888	2959	1737	1701
calix II/KCl	2861	2928	2888	2962	1739	1708
calix II/$CaCl_2$	2858	2925	2882	2950	1740	1704
calix II/$CuCl_2$	2852	2921	2873	2957	1744	1710

the modification of the intermolecular interaction between the *tert*-Bu groups upon complexation.

4. Conclusions

As shown with molecular modeling, calix II forms intramolecular complexes with mono- and divalent metal cations; divalent cations are bound 2−7 times stronger compared to monovalent cations; modeling indicates that the lowest energy structure is that shown in Figure 3A. The intramolecular complexes formed by calix I are significantly less stable compared to calix II (Table 1). Taking into account the structure of X−calix I presented in Figure 4, it can be supposed that complexation of the cation would make the corresponding ester bond more strained and labile compared to X−calix II presented in Figure 3A. On the other hand, the experimental (PM-IRRAS) results indicate that both ketone and ester C═O groups are involved in the formation of calix I and calix II complexes. In other words, both methods taken together let us think that calix I forms x−(calix $I)_2$ intermolecular complexes, while the structure of the complexes formed by calix II is that corresponding to Figure 3A; in the case of calix II, there is no evidence that intermolecular complexes are formed.

From the point of view of biological activity, it can be expected that the bulky X−(calix $I)_2$ complex may have a more perturbing effect on the cell membranes compared to the intramolecular X−calix II. Moreover, under physiological conditions, the nalidixic acid could be liberated more easily from X−(calix $I)_2$ compared to X−calix II. While the results obtained in the present study suggest that monosubstituted calixarene−antibiotic conjugates may be better candidates for antimicrobial developments, further studies using both calix I and calix II and *in vitro* cell cultures are needed to clarify the latter point.

Acknowledgment. This work was supported by a Hubert Curien partnership ("Polonium", no. 20077QA) and the Ministry of Science and Higher Education, Poland (project no. 1206/GDR/2007/03). The technical assistance of Francis Hoffmann

is gratefully acknowledged. All calculations were performed at ACK CYFRONET (grant MNiSW/SGI3700/UJ/161/2010).

References and Notes

(1) Gutsche, C. D. In Calixarenes Revisited, 1998.
(2) Lucke, A.; Stirling, C. J. M.; Bohmer, V. In *Calixarenes 2001*; Asfari, Z., Ed.; Kluwer Academic: Kluwer, Dordrecht, The Netherlands, 2001, pp 612−626.
(3) de Fatima, A.; Fernandes, S. A.; Sabino, A. A. *Curr. Drug Discovery Technol.* **2009**, *6*, 151–170.
(4) Rodik, R. V.; Boyko, V. I.; Kalchenko, V. I. *Curr. Med. Chem.* **2009**, *16*, 1630–1655.
(5) Harris, S. J. In *PCT Int. Appl.*; (Aids Care Pharma Limited, Ire.). Wo, 2002; p 44.
(6) Motornaya, A. E.; Alimbarova, L. M.; Shokova, E. A.; Kovalev, V. V. *Pharm. Chem. J.* **2006**, *40*, 68–72.
(7) Hart, P. D. A.; Armstrong, J. A.; Brodaty, E. *Infect. Immun.* **1996**, *64*, 1491–1493.
(8) Casnati, A.; Fabbi, M.; Pelizzi, N.; Pochini, A.; Sansone, F.; Ungaro, R. *Bioorg. Med. Chem. Lett.* **1996**, *6*, 2699–2704.
(9) Ben Salem, A.; Regnouf-de-Vains, J.-B. *Tetrahedron Lett.* **2003**, *44*, 6769–6771.
(10) Ben Salem, A.; Regnouf-de-Vains, J.-B. *Tetrahedron Lett.* **2001**, *42*, 7033–7036.
(11) Mourer, M.; Duval, R. E.; Finance, C.; Regnouf-de-Vains, J.-B. *Bioorg. Med. Chem. Lett.* **2006**, *16*, 2960–2963.
(12) Dibama, H. M.; Clarot, I.; Fontanay, S.; Salem, A. B.; Mourer, M.; Finance, C.; Duval, R. E.; Regnouf-de-Vains, J.-B. *Bioorg. Med. Chem. Lett.* **2009**, *19*, 2679–2682.
(13) Mourer, M.; Psychogios, N.; Laumond, G.; Aubertin, A.-M.; Regnouf-de-Vains, J.-B. *Bioorg. Med. Chem.* **2010**, *18*, 36–45.
(14) Mourer, M.; Dibama, H. M.; Fontanay, S.; Grare, M.; Duval, R. E.; Finance, C.; Regnouf-de-Vains, J.-B. *Bioorg. Med. Chem.* **2009**, *17*, 5496–5509.
(15) Grare, M.; Mourer, M.; Fontanay, S.; Regnouf-de-Vains, J.-B.; Finance, C.; Duval, R. E. *J. Antimicrob. Chemother.* **2007**, *60*, 575–581.
(16) Andersson, M. I.; MacGowan, A. P. *J. Antimicrob. Chemother.* **2003**, *51*, 1–11.
(17) Valisena, S.; Palumbo, M.; Parolin, C.; Palu, G.; Meloni, G. A. *Biochem. Pharmacol.* **1990**, *40*, 431–436.
(18) Turel, I. *Coord. Chem. Rev.* **2002**, *232*, 27–47.
(19) Polk, R. E. *Am. J. Med.* **1989**, *87*, 76S–81S.
(20) Corvis, Y.; Korchowiec, B.; Korchowiec, J.; Badis, M.; Mironiuk-Puchalska, E.; Fokt, I.; Priebe, W.; Rogalska, E. *J. Phys. Chem. B* **2008**, *112*, 10953–10963.
(21) Ishikawa, Y.; Kunitake, T.; Matsuda, T.; Otsuka, T.; Shinkai, S. *J. Chem. Soc., Chem. Commun.* **1989**, 736–738.
(22) Yagi, K.; Khoo, S. B.; Sugawara, M.; Sakaki, T.; Shinkai, S.; Odashima, K.; Umezawa, Y. *J. Electroanal. Chem.* **1996**, *401*, 65–79.
(23) Dei, L.; Casnati, A.; Lo Nostro, P.; Baglioni, P. *Langmuir* **1995**, *11*, 1268–1272.
(24) Lo Nostro, P.; Capuzzi, G.; Fratini, E.; Dei, L.; Baglioni, P. *Prog. Colloid Polym. Sci.* **2001**, *118*, 238–242.
(25) Lo Nostro, P.; Casnati, A.; Bossoletti, L.; Dei, L.; Baglioni, P. *Colloids Surf., A* **1996**, *116*, 203–209.
(26) Korchowiec, B.; Ben Salem, A.; Corvis, Y.; Regnouf de Vains, J.-B.; Korchowiec, J.; Rogalska, E. *J. Phys. Chem. B* **2007**, *111*, 13231–13242.
(27) Shahgaldian, P.; Coleman, A. W. *Langmuir* **2003**, *19*, 5261–5265.
(28) Danil de Namor, A. F.; Chahine, S.; Castellano, E. E.; Piro, O. E.; Jenkins, H. D. B. *Chem. Commun. (Cambridge, U.K.)* **2005**, 3844–3846.
(29) Frisch, M. J. T.; Trucks, G. W.; Schlegel, H. B.; Scuseria, G. E.; Robb, M. A.; Cheeseman, J. R.; Montgomery, J. A., Jr.; Vreven, T.; Kudin, K. N.; Burant, J. C.; Millam, J. M.; Iyengar, S. S.; Tomasi, J.; Barone, V.; Mennucci, B.; Cossi, M.; Scalmani, G.; Rega, N.; Petersson, G. A.; Nakatsuji, H.; Hada, M.; Ehara, M.; Toyota, K.; Fukuda, R.; Hasegawa, J.; Ishida, M.; Nakajima, T.; Honda, Y.; Kitao, O.; Nakai, H.; Klene, M.; Li, X.; Knox, J. E.; Hratchian, H. P.; Cross, J. B.; Bakken, V.; Adamo, C.; Jaramillo, J.; Gomperts, R.; Stratmann, R. E.; Yazyev, O.; Austin, A. J.; Cammi, R.; Pomelli, C.; Ochterski, J. W.; Ayala, P. Y.; Morokuma, K.; Voth, G. A.; Salvador, P.; Dannenberg, J. J.; Zakrzewski, V. G.; Dapprich, S.; Daniels, A. D.; Strain, M. C.; Farkas, O.; Malick, D. K.; Rabuck, A. D.; Raghavachari, K.; Foresman, J. B.; Ortiz, J. V.; Cui, Q.; Baboul, A. G.; Clifford, S.; Cioslowski, J.; Stefanov, B. B.; Liu, G.; Liashenko, A.; Piskorz, P.; Komaromi, I.; Martin, R. L.; Fox, D. J.; Keith, T.; Al-Laham, M. A.; Peng, C. Y.; Nanayakkara, A.; Challacombe, M.; Gill, P. M. W.; Johnson, B.; Chen, W.; Wong, M. W.; Gonzalez, C.; Pople, J. A. *Gaussian 03*, revision C.02; Gaussian, Inc.: Wallingford, CT, 2004.
(30) Vogel, V.; Moebius, D. *J. Colloid Interface Sci.* **1988**, *126*, 408–420.
(31) Vogel, V.; Moebius, D. *Thin Solid Films* **1988**, *159*, 73–81.
(32) Czapla, K.; Korchowiec, B.; Rogalska, E. *Langmuir* **2010**, *26*, 3485–3492.
(33) Wei, O.-Y.; Weis, M.; Yamamoto, T.; Manaka, T.; Iwamoto, M. *J. Chem. Phys.* **2009**, *130*, 104706/104701–104706/104707.
(34) Zawisza, I.; Bilewicz, R.; Luboch, E.; Biernat, J. F. *Dalton* **2000**, 499–503.
(35) Koelsch, P.; Viswanath, P.; Motschmann, H.; Shapovalov, V. L.; Brezesinski, G.; Moehwald, H.; Horinek, D.; Netz, R. R.; Giewekemeyer, K.; Salditt, T.; Schollmeyer, H.; Von Klitzing, R.; Daillant, J.; Guenoun, P. *Colloids Surf., A* **2007**, *303*, 110–136.
(36) Blaudez, D.; Buffeteau, T.; Cornut, J. C.; Desbat, B.; Escafre, N.; Pezolet, M.; Turlet, J. M. *Appl. Spectrosc.* **1993**, *47*, 869–874.
(37) Blaudez, D.; Turlet, J.-M.; Dufourcq, J.; Bard, D.; Buffeteau, T.; Desbat, B. *J. Chem. Soc., Faraday Trans.* **1996**, *92*, 525–530.
(38) Blaudez, D.; Buffeteau, T.; Cornut, J. C.; Desbat, B.; Escafre, N.; Pezolet, M.; Turlet, J. M. *Thin Solid Films* **1994**, *242*, 146–150.
(39) Gravier, J.; Korchowiec, B.; Schneider, R.; Rogalska, E. *Chem. Phys. Lipids* **2009**, *158*, 102–109.
(40) Lavoie, H.; Desbat, B.; Vaknin, D.; Salesse, C. *Biochemistry* **2002**, *41*, 13424–13434.
(41) Faull, J. D.; Gupta, V. K. *Thin Solid Films* **2003**, *440*, 129–137.
(42) Vanderkooi, J. M.; Dashnau, J. L.; Zelent, B. *Biochim. Biophys. Acta, Proteins Proteomics* **2005**, *1749*, 214–233.
(43) Takei, K.-i.; Takahashi, R.; Noguchi, T. *J. Phys. Chem. B* **2008**, *112*, 6725–6731.
(44) Zhang, Z.; Verma, A. L.; Yoneyama, M.; Nakashima, K.; Iriyama, K.; Ozaki, Y. *Langmuir* **1997**, *13*, 4422–4427.
(45) Wu, W.; Wang, H.-S.; Ozaki, Y. *Vib. Spectrosc.* **2009**, *50*, 285–288.
(46) Xu, Y.; Tao, J.; Xu, Z.; Weng, S.; Xu, J.; Soloway, R. D.; Wu, J.; Xu, D.; Xu, G. *Sci. China, Ser. B: Chem.* **1999**, *42*, 178–184.
(47) Sapper, H.; Cameron, D. G.; Mantsch, H. H. *Can. J. Chem.* **1981**, *59*, 2543–2549.
(48) Umemura, J.; Cameron, D. G.; Mantsch, H. H. *Biochim. Biophys. Acta, Biomembr.* **1980**, *602*, 32–44.
(49) Bakhshiev, N. G. *Opt. Spectrosc.* **2006**, *101*, 388–394.

JP102471C